HHS Public Access

Author manuscript

Exp Cell Res. Author manuscript; available in PMC 2021 June 09.

Published in final edited form as:

Exp Cell Res. 2019 January 15; 374(2): 342–352. doi:10.1016/j.yexcr.2018.12.008.

The PDZ-GEF Gef26 regulates synapse development and function via FasII and Rap1 at the *Drosophila* neuromuscular junction

Mengzhu Ou[a,1], **Su Wang**[a,1], **Mingkuan Sun**[a], **Jinsong An**[a], **Huihui Lv**[a], **Xiankun Zeng**[b], **Steven X. Hou**[b,*], **Wei Xie**[a,**]

[a]The Key Laboratory of Development Genes and Human Diseases, Ministry of Education, Institute of Life Sciences, Southeast University, Nanjing 210096, China

[b]Basic Research Laboratory, National Cancer Institute at Frederick, NIH, Frederick, MD 21702, USA

Abstract

Guanine nucleotide exchange factors (GEFs) are essential for small G proteins to activate their downstream signaling pathways, which are involved in morphogenesis, cell adhesion, and migration. Mutants of *Gef26*, a *PDZ-GEF* (PDZ domain-containing guanine nucleotide exchange factor) in *Drosophila*, exhibit strong defects in wings, eyes, and the reproductive and nervous systems. However, the precise roles of Gef26 in development remain unclear. In the present study, we analyzed the role of Gef26 in synaptic development and function. We identified significant decreases in bouton number and branch length at larval neuromuscular junctions (NMJs) in *Gef26* mutants, and these defects were fully rescued by restoring Gef26 expression, indicating that Gef26 plays an important role in NMJ morphogenesis. In addition to the observed defects in NMJ morphology, electro-physiological analyses revealed functional defects at NMJs, and locomotor deficiency appeared in *Gef26* mutant larvae. Furthermore, Gef26 regulated NMJ morphogenesis by regulating the level of synaptic Fasciclin II (FasII), a well-studied cell adhesion molecule that functions in NMJ development and remodeling. Finally, our data demonstrate that Gef26-specific small G protein Rap1 worked downstream of Gef26 to regulate the level of FasII at NMJs, possibly through a βPS integrin-mediated signaling pathway. Taken together, our findings define a novel role of Gef26 in regulating NMJ development and function.

Keywords

Gef26; Rap1; FasII; Integrin; *Drosophila*; NMJ

*Correspondence to: National Institutes of Health National Cancer Institute, Frederick, MD 21702, USA. **Correspondence to: Institute of Life Sciences, Southeast University, 2 Sipailou Road, Nanjing 210096, China. hous@mail.nih.gov (S.X. Hou), wei.xie@seu.edu.cn (W. Xie).

[1]These authors contributed equally to this work.

Conflict of interest

The authors declare that they have no conflicts of interest.

Appendix A. Supporting information

Supplementary data associated with this article can be found in the online version at doi:10.1016/j.yexcr.2018.12.008

1. Introduction

Small G proteins switch between an active, GTP-bound conformation and an inactive, GDP-bound form, thereby allowing downstream signaling pathways to be quickly turned on or off. Activation of small G proteins is facilitated by guanine nucleotide exchange factors (GEFs), which promote the binding of GTP. Specific effectors are then activated to launch the downstream signaling pathway [1]. Gef26 contains all of the conserved domains of mammalian and nematode PDZ-GEFs, including the cyclic nucleotide monophosphate-binding domain (cNMP), PDZ domain, Ras association (RA) domain and N-terminal catalytic GEF domain. It also contains a Ras exchange motif (REM), a proline-rich region (P), and a PDZ-binding motif (PBM) (Fig. S1A). There are two mammalian homologues of Gef26, RapGEF2, which has been reported to be involved in neuronal migration [2], and RapGEF6. Previous research has shown that Gef26 regulates cell mobility via integrins in the embryo [3] and cell adhesion via DE-cadherin in the reproductive system [4]. However, much less information has been reported so far on the function of Gef26 in nervous system development. Given that synapses represent a form of cell adhesion between neurons or between a neuron and another cell type, Gef26 may play an important role in synapse development as well.

The *Drosophila* NMJ consists of 30 muscles per hemi-segment repeated in each abdominal segment and 36 motor neurons (MNs) innervating these muscles accurately, and therefore, is an ideal system to study synapse development and to understand disorders of neurotransmission in mammals [5–7]. These 36 MNs bundle together in three main branches containing the transverse nerve (TN), intersegmental nerve (ISN), and segmental nerve (SN) [8]. Pioneer neurons of the ISN project away from the central nervous system and navigate through the muscle field to target specific muscles during NMJ development. The transcription factor Even-skipped (Eve) plays a critical role in determining the specific guidance characteristics of these ISN pioneer neurons [9]. Increasing studies have dissected that Eve regulated the cell adhesion molecule (CAM) FasII and Neuroglian (Nrg) expression levels in fasciculation of the MNs [10].

FasII, the *Drosophila* ortholog of mammalian neural cell adhesion molecule (NCAM), has been shown to play pivotal roles in NMJ growth and maintenance during nerve development [11]. In the absence of FasII, synapses are formed but fail to be maintained [12,13], whereas decreased levels of synaptic FasII and overexpression of FasII in both pre-neuron and post-muscle can lead to supernormal NMJ expansion. However, overexpression of FasII in either preneurons or post-muscle decreased NMJ size, which indicates that excess FasII on either side of the NMJ is essential for constraining synaptic growth [11]. Thus, there exists a linear relationship between presynaptic FasII and NMJ size, and modification—rather than elimination—of FasII levels results in a significant difference in the final size of the NMJ [13,14]. In addition to regulation of expression, local FasII level is regulated through multiple mechanisms, including integrin and mitogen-activated protein kinase (MAPK) signaling pathways [11,15–19].

Rap1, also known as Roughened in *Drosophila*, is reported to be activated by six GEFs, including Gef26 [20]. Rap1 is classified as a Ras-like small G protein because its structure is

highly analogous to that of Ras [21]. Previous research has reported that Rap1 blocks mitogenic activity in cells by silencing downstream MAPK [22,23], but that it can also activate MAPK independent of Ras during eye development and embryogenesis in *Drosophila* [8,24]. However, it remains controversial how Rap1 interacts with Ras to mediate signaling downstream of receptor tyrosine kinases. Previous studies demonstrated that PDZ-GEFs function as Rap1 activators in different tissues and organisms [25–27]. Genetic analyses showed that, in migrating macrophages, Gef26 acts upstream of Rap1 to regulate cell adhesion and cell shape via a pathway that requires the function of βPS integrins in the *Drosophila* embryo [3], but the underlying mechanism and effect of the Gef26-Rap1 pathway on integrin remain unknown.

In the present study, significant defects of NMJ morphology were detected in *Gef26* mutants, and the downstream signaling pathways responsible for this process were analyzed. Our study highlights Gef26 as a novel factor participating in NMJ growth, and shows that FasII is an essential molecule responsible for the function of Gef26 in NMJ growth. Moreover, our results indicate that Gef26 functions upstream of small G protein Rap1 to regulate local FasII level, likely through an integrin-mediated mechanism, during NMJ growth.

2. Materials and methods

Fly stocks-

All stocks were grown at 25 °C on standard medium. The wild-type (WT) *Drosophila melanogaster* strain used in this study was w^{1118}. *Elav-Gal4* (C155), *UAS-rlRNAi* (36058), and *UAS-rl* (36270) were obtained from the Bloomington Drosophila Stock Center (bdsc.india-na.edu). The *C57-Gal4* line was provided by V. Budnik (University of Massachusetts School of Medicine, Worcester, MA). $gef26^{3}$, $gef26^{6}$, $UAS\text{-}gef26^{\Delta N1}$, and *P[Gef26+]* were generated in Steven X. Hou's lab (National Institutes of Health [NIH], National Cancer Institute, Bethesda, MD). $rap1^{rv(R)B1}$ was kindly provided by I. Hariharan (Massachusetts General Hospital Cancer Center and Harvard Medical School, MA) [21]. $UAS\text{-}rap1^{V12}$ *and* $UAS\text{-}rap1^{N17}$ were the gift of Rolf Reuter (Interfaculty Institute for Cell Biology, University of Tübingen, Germany). mys^{b9} was the gift of Chunfang Wu (University of Iowa, Iowa City, IA). *UAS-fasIIRNAi* (THU2922) and *UAS-mysRNAi* (THU0581) were purchased from TsingHua Fly Center (THFC, Tsinghua University, Beijing, China).

Quantification of Gef26 mRNA and PCR-

Total RNA was extracted from intact third-instar larvae, and RT-PCR was performed with primers 5′-GACCATGTGACTAGCAAGCG-3′ and 5′-ACTTCGCACGGACTTGAAAC-3′ starting from base 1414 to base 1593 of the *Gef26* coding sequence. cDNA was prepared with HiScript II Q RT SuperMix for qPCR (+gDNA wiper) (Vazyme, Piscataway, NJ) and RT-PCR was performed with AceQ qPCR SYBR Green Master Mix (Vazyme, Piscataway, NJ).

Genomic DNA was extracted from intact adults, and PCR was performed with primers 5′-CAACGAGTTCTACCAGCGAT-3′ and 5′-AGAT CGACCGAGGGTAGAGG-3′, which

were designed based on the Gef26 coding sequence. An intron was included in the cloning fragment from the Gef26 gene region.

In situ hybridization and immunohistochemistry-

The sequence containing base 446 to base 473 of *Gef26* mRNA was PCR-amplified and cloned into pBluescript SKII (−) (Stratagene, San Diego, CA). Digoxigenin (DIG)-labeled sense and antisense RNA probes were generated in vitro with a DIG labeling kit (Roche Applied Science, Penzberg, Germany). Whole-mount in situ hybridization was performed according to standard procedures [28]. Embryos were collected for 1–2 h and further incubated at 25 °C. Embryo staging based on incubation time was according to Campos-Ortega and Hartenstein [29].

Dissection of wandering third-instar larvae and immunohistochemical analysis of the larval body wall were performed as described previously [30]. In brief, samples were blocked in phosphate-buffered saline containing 1% bovine serum albumin (BSA) at 25 °C for 1 h and incubated with primary antibody at 4 °C overnight, followed by incubation with appropriate secondary antibodies for 2 h at 25 °C. The following primary and secondary antibodies were used: rabbit anti-horseradish peroxidase (HRP) (1:500; Jackson ImmunoResearch, West Grove, PA), mouse anti-Dlg (4F3, 1:100, Developmental Studies Hybridoma Bank [DSHB], dshb.biology.uiowa.edu), mouse anti-activezone protein Bruchpilot (Brp) (nc82, 1:25, DSHB), mouse anti-βPS (CF-6G11, 1:50, DSHB), mouse anti-FasII (1D4, 1:25, DSHB), rabbit anti-Erk1/2 (1:100, Cell Signaling Technology, Danvers, MA), and rabbit anti-phospho-Erk1/2 (1:100, Cell Signaling Technology). The F-actin probe was conjugated to the red fluorescent dye rhodamine phalloidin (1:25, Invitrogen, Carlsbad, CA) and Alexa Fluor 488- or Alexa Fluor 555- conjugated to secondary antibodies (1:500, Invitrogen). Following secondary antibody incubation, the samples were washed extensively and mounted in VectaShield mounting medium (Vector Laboratories, Burlingame, CA).

Embryos of each genotype were collected simultaneously within 4 h and further incubated at 25 °C for another 16 h to ensure that most of the embryos were at stage 16/17. Stage 16/17 embryos were stained with mouse anti-FasII (1D4, 1:25, DSHB) and F-actin probe conjugated to rhodamine phalloidin (1:25, Invitrogen).

Western blots and GST pull-down-

For detecting the relative levels of Rap1-GTP, an active Rap1 pull down and detection kit (no. 16118; Thermo Scientific, Waltham, MA) was used. The procedure for western blot analysis has been described previously [30]. Briefly, adult *Drosophila* heads were homogenized in 1× SDS loading buffer. Protein lysates were separated on a 12% SDS-polyacrylamide gel and electro-transferred onto polyvinylidene difluoride membranes. Membranes were blocked in Tris-buffered saline containing 3% BSA (BioFroxx, Einhausen, Germany) at 25 °C for 2 h. Proteins immobilized on the membrane were probed with primary antibodies at 4 °C overnight. The primary antibody used for western blot analysis was rabbit anti-Rap1 (1:250, Thermo Scientific, Waltham, MA). Samples were then incubated with HRP-conjugated secondary antibody at 25 °C for 1 h, and the targeted

proteins were visualized with the Qentix Western Blot Signal Enhancer and SS West Pico Substrate Detection System (Thermo Scientific).

The GST pull-down assay was performed with an active Rap1 Pull-Down and Detection Kit (Thermo Scientific) and the whole procedure was conducted according to the kit instructions.

Electrophysiology-

Conventional intracellular recordings were used for assessing NMJ neurotransmission [31]. Wandering third-instar larvae were dissected in Ca^{2+}-free HL3.1 saline. Gut and fat were removed, and the body wall was spread out to expose the nerves and muscles. Microelectrodes (20–50 MΩ) were pulled from borosilicate glass (WPI, Sarasota, FL) with a glass puller (P-2000; Sutter Instruments, Novato CA) and filled with 3 M KCl. Recordings were performed at 25 °C with an Axoclamp 2B amplifier (Molecular Devices, San Jose, CA) in bridge mode. Recording data were digitized with a Digitizer 1322A (Molecular Devices) and collected using pClamp 9.1 software (Molecular Devices). For excitatory junction potential (EJP) recordings, the SN was cut, and the free end was drawn into a microelectrode and stimulated with a Grass S48 stimulator (Astro-Med, Artisan Technology Group, Champaign, IL) at 0.3 Hz with suprathreshold stimulating pulse. Both EJPs and miniature EJPs (mEJPs) were recorded from muscle 6 of abdominal segment A3 in HL3.1 saline containing 0.8 mM Ca^{2+} and/or 0.6 mM Ca^{2+}. Three EJP responses were collected for each animal, and mEJPs were recorded for a period of 60 s after the EJP recording. Data was processed with Mini Analysis software (Synaptosoft, Decatur, GA) and statistically evaluated with SigmaPlot software. Only recordings with resting membrane potentials ranging from − 65 to − 75 mV were used for analysis.

Larval locomotor activity detection-

The larval locomotion assay was performed as described [32]. Individual larvae were placed in the center of transparent dishes 15 cm in diameter containing 3% agar. The agar was stained dark purple by addition of a minute amount of food coloring. The movement of the larvae was visualized using a standard commercial video camera, and the trajectory over 3 min and/or 30 s was tracked by tracker software written in Python. Three-minute and/ or thirty-second trajectory distances were calculated to assess larval locomotor activity.

Image analysis-

Images were collected using a Carl Zeiss LSM 710 confocal station and analyzed with ImageJ software (NIH). For quantification of bouton number and branch length, dissected body wall muscle samples were stained with anti-HRP and anti-Dlg antibodies, and the NMJs of muscle 4 and 6/7 of abdominal segments 2 and 3 were collected. For quantification of bouton number, type Ib boutons at NMJ6/7 were collected and manually counted. Branch length was measured using Image J and average branch length was calculated for each NMJ. For embryo ISN projections at embryonic stage 16/17, embryos were stained with anti-FasII antibody and phalloidin. Total ISN defects, including ISN bifurcation and ISN early stall, were manually counted, and ratios calculated in A2–A6 abdominal hemi-segments in different genetic backgrounds. For quantification of fluorescence intensity, type Ib boutons

at NMJ4 were measured using ImageJ software. For comparison of fluorescence intensity between genotypes, all samples were dissected and fixed under identical conditions, processed in the same vials and collected under the same microscope setting. All assays were replicated at least three times. For each channel, the sum of pixel intensities was recorded using ImageJ. We used anti-HRP staining as internal reference [30,33]. The ratios of Brp/HRP, βPS/HRP and FasII/HRP intensity were calculated for each genotype.

All experiments and analyses were performed blind with respect to the genotypes used whenever possible. All the averaged data in this study are reported as mean ± SEM. $p < 0.05$ was considered statistically significant. Statistical significance was determined using Student's *t*-test for comparisons of two groups. *p* values are indicated in figure legends.

3. Results

Loss of Gef26 results in impaired NMJ morphology-

To investigate the function of Gef26 in vivo, two *Gef26* mutants were utilized. In $gef26^3$, the P element *l(2)SH1450* was inserted into the 5′ promoter sequence of the gene encoding Gef26, 846 bp away from the ATG translation start site. The phenotype and lethality associated with *l(2)SH1450* was reverted to WT by the mobilization of the P element. The $gef26^6$ allele contains a 3-kb deletion surrounding the *l(2)SH1450* insertion site, including the first two exons of *Gef26* and a large 5′ segment of the third (Fig. S1B). Significantly decreased *Gef26* transcript levels were detected in $gef26^3$ and $gef26^6$ (Fig. S1C).

To examine the function of Gef26 in the NMJ, we used the pan-neuronal presynaptic marker HRP and postsynaptic subsynaptic reticulum (SSR) marker discs large 1 (Dlg) to investigate NMJ morphology. To facilitate quantitative analysis, we focused on type Ib boutons at NMJ6/7 of abdominal segment 2/3. Apparent NMJ morphological defects in *Gef26* mutants were observed (Fig. 1A-C, S2A-D) and statistical analyses showed significantly decreased bouton number and branch length at NMJ6/7 of each mutant compared with WT (Fig. 1F-G, S2F-G). To ascertain whether the decreased bouton number and branch length were attributed to *Gef26* deficiency, we introduced *P [Gef26+]*, which is predicted to contain the complete *Gef26* coding region (Fig. S1B) in the *Gef26* mutant lines. Transcription levels of *Gef26* were restored almost to WT level (Fig. S1C). When expressing full-length Gef26 using *P[Gef26+]* in the $gef26^3$ and $gef26^6$ mutant backgrounds, previously observed defects of *Gef26* mutants were almost fully rescued (Fig. 1E-G, S2E-G). These results indicate that Gef26 is essential for normal NMJ morphology. A dominant-negative form of *Gef26*, $gef26^{\Delta N1}$, was generated by expressing a construct in which part of the N-terminal portion of the protein (from the second to the last amino acid of the cNMP domain) was deleted (Fig. S1A). To identify $UAS\text{-}gef26^{\Delta N1}$, a pair of primers was designed to clone a *Gef26* coding sequence fragment that contains an intron of *Gef26* genomic DNA. Two bands were cloned from the $gef26^{\Delta N1}$ transgene and *Gef26* genomic DNA in the $UAS\text{-}gef26^{\Delta N1}$ line, whereas only one band was generated using WT DNA as template, confirming the transgenetic fly (Fig. S1D). Further, rough eyes were observed in $UAS\text{-}gef26^{\Delta N1}$ driven by pan–-neuron-specific *Elav-Gal4*, which was consistent with *Gef26* mutants reported before (27). This phenotype indicated that expression of $gef26^{\Delta N1}$ was sufficient to block the function of Gef26. Blocking the function of Gef26 by *Elav-Gal4*-driven expression of

dominant-negative *gef26*$^{\Delta N1}$ resulted in defects similar to those of *Gef26* mutants (Fig. 1B-C, H-O, S2B-D). However, *gef26*$^{\Delta N1}$ driven by muscle-specific *C57-Gal4* did not mimic the mutant phenotype. These results indicate that Gef26 in presynaptic neurons rather than in postsynaptic muscle is required for normal NMJ morphology.

Gef26 functions during NMJ development-

During NMJ development, MNs innervate the muscles at the end plate, and the axon terminals branch into fine synaptic varicosities that insert into the folds of the muscle membrane. Thus, the boutons form as clusters of synapses between MNs and muscle. Many larval-born neurons undergo remodeling during morphogenesis so that NMJs are subject to spouting as well as pruning of boutons during development [34,35]. As a result, NMJs undergo an approximately 10-fold increase in synaptic bouton number during the three larval stages [12,36].

The severe decrease in bouton number and branch length at an NMJ in the third-instar larval stage caused by loss of Gef26 might trace back to an earlier developmental stage. Using RNA in situ hybridization we first confirmed the spatial distribution of the *Gef26* transcript at different stages in the embryo, and we observed that Gef26 is highly expressed in the nervous system from embryonic stage 13–16 (Fig. 2A-F). Furthermore, to examine whether Gef26 has an effect on NMJ development in earlier larval stages, we examined second-instar larvae and detected decreased bouton number and branch length in *Gef26* mutant compared to WT (Fig. 2G-I, K-L), similar to that seen in third-instar larvae. Consistently, these defects were significantly rescued when *P [Gef26+]* was introduced into *Gef26* mutant line (Fig. 2J, K-L). These results indicated that Gef26 was involved in NMJ development.

Loss of Gef26 leads to functional defects-

Given that defects in NMJ morphology frequently disrupt normal function, it was conceivable that the severe defects of NMJ morphology in *Gef26* mutants might impair NMJ function. To confirm this hypothesis, we first examined function by visualizing the active zone as marked by the Brp protein, but no significant difference was observed (Fig. S3D-F). Then electro-physiological recordings were performed at NMJ6/7 of the third-instar larvae under approximately physiological conditions with HL3.1 containing 0.6 mM Ca^{2+}. The mean amplitudes of EJPs in larvae were significantly decreased in *gef26*^{3} and *gef26*^{3}/*gef26*^{6} compared to WT, and such a decrease could be rescued by *P[Gef26+]* (Fig. 3A, C). Interestingly, the frequency of mEJPs showed no significant difference between mutants and WT (Fig. 3B, D). These results are evidence that the functional defects of NMJs were indeed due to loss of Gef26. It appears that the functional defect was due to reduced bouton number rather than the capacity of individual boutons. We then hypothesized that functional defects of NMJs would cause behavioral impairment. Hence, larval locomotor activity was assessed in all of the *Gef26* mutants as well as WT larvae. Compared with WT, both *gef26*^{3} and *gef26*^{3}/ *gef26*^{6} mutant flies showed reduced locomotor activity. This behavioral defect was also rescued by *P[Gef26+]* (Fig. 3E). Together, these results indicate that Gef26 is required for normal NMJ function and locomotor activity.

However, no significant change was observed in *gef26*^{6} in the functional test. Nonetheless, a slight tendency to decreased function could be observed compared to WT (Fig. 3A, C). We then increased the physiological EJP amplitude by increasing the concentration of Ca^{2+} to 0.8 mM and extending locomotion testing time to 3 min. EJP amplitude was significantly decreased in *gef26*^{6} compared to WT (Fig. S3A-B). Compared with WT, *gef26*^{6} also showed reduced locomotor activity in the 3-min test (Fig. S3C). Furthermore, blocking the function of Gef26 by *Elav-Gal4*-driven *gef26*$^{\Delta N1}$ resulted in both decreased EJP amplitude with 0.8 mM Ca^{2+} (Fig. S3G, I) and reduced locomotor activity in the 3-min test similar to *Gef26* mutants (Fig. 4N; Fig. 5O), while no significant difference of mEJP frequency was detected (Fig. S3H, J).

Increased FasII is responsible for defective NMJ morphology with loss of Gef26-

Having shown that Gef26 is involved in NMJ development, we looked for NMJ defects at an early development stage and examined the ISN phenotype of stage 16/17 embryos using anti-FasII antibody and phalloidin to visualize the pattern and relative position of motor axons, as well as their target muscles. Because abnormal motor axon-guidance phenotypes were observed in *Gef26* mutants, the proportion of hemi-segments demonstrating defects, including early stalls and bifurcations as previously reported [10,37], was quantified in different genetic backgrounds. Significantly increased ISN defects were observed in *gef26*^{3} (59.5%), *gef26*^{6} (37.5%), and *gef26*^{3}/*gef26*^{6} (47%), whereas only 6.286% of WT hemisegments showed defects (Fig. S4A-H). These defects were similar to those observed in the *FasII* mutant, which suggested a potential connection between Gef26 and FasII in NMJ development.

Several CAMs have been implicated to function in synapse growth and plasticity [38]. Among them, FasII is a typical synaptic remodeling CAM in *Drosophila*. FasII-mediated regulation of synapse growth and maintenance is reflected in the change in NMJ size in FasII mutants or FasII-overexpressing flies. As the level of synaptic FasII is critical for NMJ size, we first examined the local FasII level at NMJs in *Gef26* mutants. As similar defects were observed at NMJ4 in *Gef26* mutants (Fig. S5F-G) and the brief frame of NMJ4 made it clear to distinguish the difference, we used NMJ4 for further protein level investigation. FasII level was significantly increased in *gef26*^{3} (Fig. 4B, E), which was consistent with the decreased bouton number in *Gef26* mutants and FasII overexpression alleles described in previous studies. The increased FasII could also be reduced to WT level by *P[Gef26+]* rescue (Fig. 4D, E). These results indicate that increased FasII at NMJs is responsible for the shrinking NMJ size in *Gef26* mutants.

To confirm that Gef26 controls NMJ growth through affecting FasII level at NMJs, we attempted to rescue NMJ defects caused by defective Gef26 by genetic reduction of synaptic FasII level. According to previous research, although FasII is mainly derived from neurons, it clusters both pre- and post-synapse at NMJs, and either or both conditions could affect NMJ morphology. As it was shown that Gef26 acts at neurons, further research would be focused pre-synapse. *Elav-Gal4*-driven *fasIIRNAi* effectively reduced FasII level, and expressing *gef26*$^{\Delta N1}$ in neurons increased FasII level at NMJs as seen in *Gef26* mutants (Fig. S5A-E). To investigate whether increased clustering of presynaptic FasII was

responsible for the NMJ defects caused by lack of Gef26, we expressed *fasIIRNAi* together with *Elav-Gal4*–driven $gef26^{\Delta N1}$ in neurons and observed considerable rescue of the NMJ defects, including decreased bouton number and branch length (Fig. 4L-M). The reduced locomotor activity in *Elav-Gal4*–driven $gef26^{\Delta N1}$ could also be rescued by expressing *fasIIRNAi* simultaneously (Fig. 4N). These results indicate that normal presynaptic FasII level is responsible for Gef26 function in NMJ growth.

Gef26 targets Rap1 in Drosophila NMJ morphogenesis-

The small G protein Rap1 has been proven to be crucial in development due to its roles in cell migration and adhesion-junction formation in *Drosophila*. Previous studies reported that Gef26 functions as the upstream activator of Rap1, and that this activation is involved in physiological processes including dorsal closure, wing development, stem-cell maintenance in spermatogenesis and macrophage migration, and eye and ovary development [4,27,39,40].

To investigate whether Rap1 was the target of Gef26 in NMJ development, we first examined the phenotype of *Rap1* mutant $rap1^{rv(R)B1}$. Loss of Rap1 led to decreased bouton number and branch length similar to that seen in *Gef26* mutants (Fig. 5A-C, E-F). To determine whether Rap1 and Gef26 function in NMJ growth in the same pathway, we next examined whether the defects in the *Rap1* mutant would be aggravated by reducing Gef26 at the same time. Double mutants of *Gef26* and *Rap1* did not show enhanced NMJ defects compared to any single mutant of *Gef26* or *Rap1* (Fig. 5D, E). These results suggested that Rap1 and Gef26 act on the same pathway to regulate NMJ growth. To further investigate whether Gef26 targets Rap1 in NMJ growth, we tested the ability of activated Rap1 to restore NMJ size. When we expressed the constitutively active form of Rap1 ($rap1^{V12}$) [3], in which Rap1 was activated independent of Gef26, together with dominant-negative $gef26^{\Delta N1,}$ in neurons, the NMJ defects caused by blocking Gef26 were rescued to a certain extent (Fig. 5G-N). The reduced locomotor activity in *Elav-Gal4*–driven $gef26^{\Delta N1}$ could also be rescued by expressing $rap1^{V12}$ simultaneously (Fig. 5O) Together these results indicate that Gef26 functions in NMJ morphogenesis by activating Rap1.

Gef26 regulates Rap1 activity in nerves-

To investigate whether Gef26 targets Rap1 in NMJ development via activating Rap1 directly, we performed GST pull-down assays to monitor Rap1 activation while blocking Gef26. Like other small GTPases, Rap1 (~ 21 kDa in *Drosophila*) is active when bound to GTP and inactive when bound to GDP. The active form of Rap1 interacts with downstream effectors such as RalGDS. Furthermore, binding of Rap1 to the Rap1-binding domain (RBD) of RalGDS inhibits intrinsic and GTPase-activating protein (GAP)-enhanced Rap1 GTPase activity. Therefore, the RalGDS-RBD can be used as a probe to specifically isolate active Rap1.

The kit we used provides a GST-fusion protein of the Rap1-binding domain (RBD) from human RalGDS, glutathione agarose resin to specifically pull down active Rap1, and an anti-Rap1 antibody for western blot detection (Fig. 6A). GST-fused Rap1-RBD efficiently pulled down activated Rap1 (Rap1-GTP) after treatment with kit GTP, but not after treatment with GDP. Significant reduction of Rap1 specific for Rap1-GTP was observed when expressing

the dominant-negative form of Gef26 in neurons compared to the control (Fig. 6B). This result indicates that Gef26 participates in Rap1 activation. Note that the anti-Rap1 provided in the kit was not prepared using *Drosophila* Rap1; therefore, the banding of Rap1 would be much more specific through specifically pulling down by GST-fusion protein of the Rap1-binding domain (RBD).

Previous studies had shown that Rap1 mutants sometimes show a far weaker phenotypic defect than *Gef26* mutants, which could be a consequence of compensation by the maternal contribution. However, expressing the dominant-negative form of Rap1, $rap1^{N17}$, resulted in a stronger phenotype [3]. To further confirm that Rap1 activity is required in NMJ morphogenesis, we also tested the $rap1^{N17}$ phenotype at NMJs when expressed in neurons. Significantly decreased bouton number and branch length (Fig. 6C-F) as well as increased FasII level at NMJs were observed (Fig. 6G-I), in accordance with that seen in *Gef26* mutants.

Gef26 regulates FasII level at NMJs by reducing integrin there-

To further investigate how the Gef26-Rap1 pathway regulates FasII level at the NMJ, we first attempted to discover the relationship between Gef26-Rap1 signaling and the Ras-MAPK pathway because Rap1 shares strong structural similarity to Ras. To assess the pErk level at NMJs, we performed immunohistochemistry. A previous study reported that phospho-ERK localizes to the active zone, which would suggest a direct mechanism [19]. However, neither Wairkar et al. nor we could replicate these localization findings [41]. We observed a quite weak signal of phosphorylated Erk at NMJs (data not shown). Further, we did not observe significantly decreased bouton number or branch length similar to that in *Gef26* or *Rap1* mutants by knocking down or overexpressing Rl (the gene encoding Erk) in neurons (Fig. S6G-L). Thus, the MAPK pathway might not be locally involved in Gef26-Rap1 signaling-mediated regulation of synaptic FasII distribution at the NMJ.

On the other hand, decreased levels of βPS integrin at the NMJ were observed in *Gef26* mutants and could be restored by *P[Gef26+]* (Fig. 7A-E). Blocking Gef26 or Rap1 in neurons resulted in a similar decrease (Fig. 7J-N). This finding indicated that integrin level at the NMJ was reduced with loss of Gef26 or Rap1 function, and further derepressed synaptic FasII, leading to reduced bouton number and branch length. Moreover, knockdown of Mys (the gene encoding βPS) by expressing *mysRNAi* in neurons also inhibits NMJ growth (Fig. S6A-F), which is consistent with the NMJ phenotype of *Gef26* and *Rap1* mutants. *Elav-Gal4*–driven *mysRNAi* indeed clearly reduced presynaptic βPS integrin in axons (Fig. 7H-I, white arrow). A classic *Mys* mutant, mys^{b9}, with low expression of βPS integrin at NMJs (Fig. 7G), also mimicked the phenotype of *Gef26* mutants. Increased FasII level at NMJs was also observed in both *mysRNAi* and mys^{b9} mutants (Fig. S7A-E), which is in accordance with observations when Gef26 or Rap1 was blocked. These results support the hypothesis that Gef26-Rap1 signaling regulates local FasII level at the NMJ, possibly through an integrin-mediated mechanism (Fig. S7F).

4. Discussion

Previous studies demonstrated that the *Drosophila* PDZ-GEF Gef26 is involved in cell morphogenesis and migration. Subsequent studies showed that the Ras-like small G protein Rap1 functions as a target of Gef26, and that Rap1 was the well-studied Gef26 specific small GTPase. In this study we discovered that Gef26 plays a pivotal role in larval NMJ morphogenesis via activating Rap1, and showed that FasII, a well-known CAM participating in NMJ development, is responsible for this process. This is consistent with the observation that defects emerge in earlier larval stages, or even in the late embryonic period, with loss of Gef26. Furthermore, integrin-mediated regulation of FasII is involved in this signaling pathway.

In addition to the defects observed in *Gef26* homozygous mutants, similar phenotypes were detected in *Gef26* heterozygous mutants, and decreased branch length was observed in the Gef26 flies overexpressing *P[Gef26+]*. These results suggest that the proper physiological level of Gef26 is essential for normal NMJ morphology. Because both *Rap1* heterozygous mutant and *Rap1* dominant-negative flies showed abnormal NMJs, the amount of functional Gef26 might affect the quantity of activated Rap1 to regulate NMJ growth. As a result, decreases in both activated Rap1 and NMJ defects were observed in neurons expressing $gef26^{\Delta N1}$.

FasII is a CAM participating in NMJ morphogenesis. Expression patterns of Gef26 in embryos revealed a concentration in nerves, suggesting that it functions in nervous system development, possibly synaptogenesis, similar to FasII. In *Gef26* mutants, immunohistochemical analysis of late-stage embryos using anti-FasII showed axon-guidance defects similar to those seen in *fasII* mutants. A previous study showed similar axon-guidance defects in embryos neuronally expressing dominant-negative and constitutive-active forms of Rap1 [42]. These results compelled us to associate the NMJ defects of *Gef26* mutants with FasII. According to published studies on the relationship between Gef26 and CAMs and similar phenotypes of the mutants of their genes, FasII very likely plays a critical role during the function of Gef26 in NMJ development. More experiments were conducted to confirm the link between these two genes in this research. However, we observed no significant difference in bouton number in FasII knockdown flies, although synaptic FasII was indeed decreased at the NMJ. According to Beck et. al. [43], a change in the relative level of the FasII-specific isoform and the pre- to post-synaptic FasII ratio, rather than a uniform reduction in FasII levels, can produce aberrant synaptic morphology. Another study showed that enhancement of new synapse formation depends on a balance of FasII levels at both sides of the synapse rather than a change in absolute levels [44]. Thus, the phenotype might depend on the actual effects of RNAi in vivo.

As genes upstream of FasII, such as Eve, were shown to control ISN guidance, there might be some interactions between Gef26 and Eve or between Eve and other signaling molecules. In actuality, FasII is more important in synapse stabilization and destabilization than in initial aspects of synaptogenesis. Although our results demonstrate their connection to NMJ growth, the possibility still exists that Gef26 functions in NMJ growth through other CAMs or molecules, possibly even targeting another small G protein and employing additional

mechanisms. Thus, more molecules and mechanisms remain to be identified to clarify how Gef26 functions on NMJ growth.

Erks are involved in a wide range of neuronal functions including differentiation, synaptic plasticity, survival, and migration [45]. Koh et al. demonstrated that the Ras-MAPK signal transduction pathway regulates synaptic plasticity through FasII-mediated cell adhesion [19]. According to their findings, the level of FasII protein at NMJs can be regarded as a sensitive readout of Ras signaling level. RapGEF2 has been shown to interact with an internalized neurotrophin receptor, which is transported to late endosomes to induce sustained activation of both Rap1 and Erk, as well as neurite outgrowth [46]. Further, Gef26 targets Rap1 to activate Erk in R7 photoreceptor specification in *Drosophila* [24]. However, we did not observe any alteration in local phosphorylation of Erk at NMJs or any defect of NMJs with Rl knockdown or overexpression, suggesting that Gef26-Rap1 might not function through MAPK signaling to regulate synaptic FasII level. However, in spite of FasII downregulation by MAPK pathway activation, other studies have demonstrated that MAPK may also regulate NMJ growth by nuclear translocation in the presynaptic cell to initiate transcription of genes required for new synapse formation [47]. Therefore, MAPK signaling in NMJ growth cannot be entirely excluded as one potential mechanism in this working model.

A number of molecules related to Gef26 and/or Rap1 have been identified in other species or systems and provide us some potential candidates for further study. In addition to established relevance we are going to look for more novel details of Gef26 function at the NMJ. Gef26 is the only PDZ-GEF in *Drosophila*, and the PDZ domain is a general domain responsible for specific protein-protein interactions. The Gef26 PDZ domain indicates potential connections with proteins containing a PBM. This may offer a critical clue for exploring new partners in Gef26-mediated regulation of NMJ growth. Until recently, the upstream signal of Gef26 and mechanism of action remained to be unidentified. In our research, the dominant-negative form of Gef26 without the cyclic nucleotide-binding domain showed a similar phenotype at NMJs to *Gef26* mutants when expressed in neurons to compete with normal Gef26, indicating that the cyclic nucleotide-binding domain is required for the proper function of Gef26 in NMJ morphogenesis, likely by binding to cAMP to receive upstream signaling. Other signaling pathways involved in NMJ development, such as the bone morphogenetic protein (BMP) and Wnt-family pathways, might also be associated with Gef26. Retrograde BMP signaling controls synaptic growth at the NMJ by regulating Trio, another GEF, in MNs [48]. According to our genetic analysis (data not shown), Gef26 may interact with these signaling pathways as well. More evidence is needed to elucidate the relationships among these pathways.

The identitiy of the direct effector of Rap1 in this model is still unclear. We have not identified a molecule through which Gef26-Rap1 acts on integrin to regulate local FasII level. Evidence to demonstrate a physiological interaction between those molecules and Rap1 is lacking, and information on downstream molecules of Rap1 is limited. Use of methods of screening based on specific phenotypes may facilitate the search for these targets in the future.

This research demonstrates that Gef26-Rap1 signaling plays an important role in NMJ growth and physiological function. These findings provide new insights into neuron innervation in NMJ development and function, and will potentially contribute to development of treatments for various neuromuscular disorders associated with defective NMJ structure or function. Finally, copy number variants of RapGEF2 and RapGEF6 have been identified in schizophrenia patients [49,50]. Therefore, it will be of interest to explore the function of Gef26 in that and other psychiatric disorders.

Supplementary Material

Refer to Web version on PubMed Central for supplementary material.

Acknowledgments

We thank Drs. Zhengping Jia and Junhai Han for useful discussions and critical comments on the manuscript; Dr. Rolf Reuter of the Bloomington Stock Center for providing *Drosophila* stocks; and the members of the Xie laboratory for their critical comments on the manuscript.

Funding: This work was supported by the National Natural Science Foundation of China (30928014 to SH, 31430035 to WX), and National Basic Research Program of China (973 Program) (2012CB517903 to WX).

Abbreviations:

GEF	Guanine nucleotide exchange factor
GAP	GTPase-activating protein
cNMP	cyclic nucleotide monophosphate-binding protein
REM	Ras exchange motif
PDZ	PSD-92/DLG/ZO-1
RA	Ras association
dPDZ-GEF	*Drosophila* PDZ domain-containing guanine nucleotide exchange factor
NMJ	neuro-muscular junction
EJP	evoked junction potential
mEJP	miniature excitatory junction potential
DLG	discs large 1
HRP	Horseradish peroxidase
MAPK	mitogen-activated protein kinase
ERK	extracellular signal-regulated kinase
MN	motor neuron

TN	transverse nerve
ISN	intersegmental nerve
SN	segmental nerve
CAM	cell adhesion molecule
FasII	Fasciclin II
Nrg	Neuroglian
NCAM	neural cell adhesion molecule
CAMKII	Ca^{2+}/calmodulin-dependent protein kinase II
PS	position specific
SSR	subsynaptic reticulum
FB	first branch point
SB	second branch point
TB	third branch point
RBD	Rap1-binding domain

References

[1]. Bos JL, Rehmann H, Wittinghofer A, GEFs and GAPs: critical elements in the control of small G proteins, Cell 129 (5) (2007) 865–877. [PubMed: 17540168]

[2]. Ye T, et al., Cdk5-mediated phosphorylation of RapGEF2 controls neuronal migration in the developing cerebral cortex, Nat. Commun 5 (2014) 4826. [PubMed: 25189171]

[3]. Huelsmann S, The PDZ-GEF dizzy regulates cell shape of migrating macrophages via Rap1 and integrins in the Drosophila embryo, Development 133 (15) (2006) 2915–2924. [PubMed: 16818452]

[4]. Wang H, et al., Rap-GEF signaling controls stem cell anchoring to their niche through regulating DE-cadherin-mediated cell adhesion in the drosophila testis, Dev. Cell 10 (1) (2006) 117–126. [PubMed: 16399083]

[5]. Koh YH, Gramates LS, Budnik V, Drosophila larval neuromuscular junction: molecular components and mechanisms underlying synaptic plasticity, Microsc. Res. Tech 49 (1) (2000) 14–25. [PubMed: 10757875]

[6]. Martinez TL, et al., Survival motor neuron protein in motor neurons determines synaptic integrity in spinal muscular atrophy, J. Neurosci 32 (25) (2012) 8703–8715. [PubMed: 22723710]

[7]. Eguchi T, Miyoshi S TT, Yamanashi Y, Molecular mechanisms underlying the formation and maintenance of neuromuscular junctions and a possible therapeutic approach, Clin. Calcium 27 (3) (2017) 413–419. [PubMed: 28232656]

[8]. Mishra S, et al., Ras-independent activation of ERK signaling via the torso receptor tyrosine kinase is mediated by Rap1, Curr. Biol 15 (4) (2005) 366–370. [PubMed: 15723799]

[9]. Landgraf M, et al., even-skipped determines the dorsal growth of motor axons in Drosophila, Neuron 22 (1) (1999) 43–52. [PubMed: 10027288]

[10]. Zarin AA, et al., A transcription factor network coordinates attraction, repulsion, and adhesion combinatorially to control motor axon pathway selection, Neuron 81 (6) (2014) 1297–1311. [PubMed: 24560702]

[11]. Packard M, Mathew D, Budnik V, FASt remodeling of synapses in Drosophila, Curr. Opin. Neurobiol 13 (5) (2003) 527–534. [PubMed: 14630214]

[12]. Schuster CM, et al., Genetic dissection of structural and functional components of synaptic plasticity. I. Fasciclin II controls synaptic stabilization and growth, Neuron 17 (4) (1996) 641–654. [PubMed: 8893022]

[13]. Schuster CM, et al., Genetic dissection of structural and functional components of synaptic plasticity. II. Fasciclin II controls presynaptic structural plasticity, Neuron 17 (4) (1996) 655–667. [PubMed: 8893023]

[14]. Stewart BA, et al., Homeostasis of synaptic transmission in Drosophila with genetically altered nerve terminal morphology, J. Neurosci 16 (12) (1996) 3877–3886. [PubMed: 8656281]

[15]. Beumer K, et al., Integrins regulate DLG/FAS2 via a CaM kinase II-dependent pathway to mediate synapse elaboration and stabilization during postembryonic development, Development 129 (14) (2002) 3381–3391. [PubMed: 12091308]

[16]. Pei-I Tsai MW, Kao Hsiu-Hua, Cheng Ying-Ju, Lin Yu-Jing, Chen Ruey-Hwa, Chien Cheng-Ting, Activity-dependent retrograde laminin A signaling regulates synapse growth at Drosophila neuromuscular junctions, PNAS 103 (43) (2012) 17699–17704.

[17]. Lee JYG, J.H, Activity-induced synaptic structural modifications by an activator of integrin signaling at the Drosophila neuromuscular junction, J. Neurosci 37 (12) (2017) 3246–3263. [PubMed: 28219985]

[18]. Pei-I Tsai MWH-HK, Cheng Ying-Ju, Walker James A., Chen Ruey-Hwa, Chien Cheng-Ting, Neurofibromin mediates FAK signaling in confining synapse growth at Drosophila neuromuscular junctions, J. Neurosci 32 (47) (2012) 16971–16981. [PubMed: 23175848]

[19]. Koh YH, et al., The Ras1-mitogen-activated protein kinase signal transduction pathway regulates synaptic plasticity through fasciclin II-mediated cell adhesion, J. Neurosci 22 (7) (2002) 2496–2504. [PubMed: 11923414]

[20]. Pannekoek W-J, et al., Cell–cell junction formation: the role of Rap1 and Rap1 guanine nucleotide exchange factors, Biochim. Biophys. Acta 1788 (4) (2009) 790–796. [PubMed: 19159611]

[21]. Asha H, Nancy D, Ruiter D, The Rap1 GTPase functions as a regulator of morphogenesis in vivo, EMBO J 18 (3) (1999) 605–615. [PubMed: 9927420]

[22]. Simon JC, Bonnee Rubinfeld IA, Frank M, RapV12 antagonizes Ras-dependent activation of ERK1 and ERK2 by LPA and EGF in rat-1 fibroblasts, EMBO J 12 (9) (1993) 3475–3485. [PubMed: 8253074]

[23]. Ishimaru S, Williams R, Activation of the Drosophila C3G leads to cell fate changes and overproliferation during development, mediated by the RAS–MAPK pathway and RAP1, EMBO J 18 (1) (1999) 145–155. [PubMed: 9878058]

[24]. Mavromatakis YE, Tomlinson A, The role of the small GTPase Rap in Drosophila R7 photoreceptor specification, Proc. Natl. Acad. Sci. USA 109 (10) (2012) 3844–3849. [PubMed: 22355117]

[25]. Rooij Jd, et al., PDZ-GEF1, a guanine nucleotide exchange factor specific for Rap1 and Rap2, J. Biol. Chem 274 (53) (1999) 38125–38130. [PubMed: 10608883]

[26]. Knox AL, Rap1 GTPase regulation of adherens junction positioning and cell adhesion, Science 295 (5558) (2002) 1285–1288. [PubMed: 11847339]

[27]. Lee JH, et al., Drosophila PDZ-GEF, a guanine nucleotide exchange factor for Rap1 GTPase, reveals a novel upstream regulatory mechanism in the mitogen-activated protein kinase signaling pathway, Mol. Cel. Biol 22 (21) (2002) 7658–7666.

[28]. Vosshall L, Wong A, Axel R, An olfactory sensory map in the fly brain, Cell 102 (2) (2000) 59–147.

[29]. Campos-Ortega JA, Hartenstein V, The Embryonic Development of Drosophila Melanogaster, 2nd ed., Springer, Berlin; New York, 1997, p. 405 (xvii).

[30]. Sun M, et al., Neuroligin 2 is required for synapse development and function at the Drosophila neuromuscular junction, J. Neurosci 31 (2) (2011) 687–699. [PubMed: 21228178]

[31]. Jan L, Jan Y, Properties of the larval neuromuscular junction in Drosophila melanogaster, J. Physiol 262 (1) (1976) 189–214. [PubMed: 11339]

[32]. Gan GXG, Drosophila Neuroligin3 regulates neuromuscular junction development and synaptic differentiation, J. Biol. Chem 289 (46) (2014) 31867–31877. [PubMed: 25228693]

[33]. Wang D, et al., Drosophila twinfilin is required for cell migration and synaptic endocytosis, J. Cell Sci 123 (Pt9) (2010) 1546–1556. [PubMed: 20410372]

[34]. Truman JW, Metamorphosis of the central nervous system of Drosophila, J. Neurobiol 21 (7) (1990) 1072–1084. [PubMed: 1979610]

[35]. Yu F, Schuldiner O, Axon and dendrite pruning in Drosophila, Curr. Opin. Neurobiol 27 (2014) 192–198. [PubMed: 24793180]

[36]. Gorczyca M, Augart C, Budnik V, Insulin-like receptor and insulin-like peptide are localized at neuromuscular junctions in Drosophila, J. Neurosci 13 (9) (1993) 3692–3704. [PubMed: 8366341]

[37]. Chavis P, Westbrook G, Integrins mediate functional pre-and postsynaptic maturation at a hippocampal synapse, Nature 411 (2001) 317–321. [PubMed: 11357135]

[38]. Murase S, Schuman EM, The role of cell adhesion molecules in synaptic plasticity and memory, Curr. Opin. Cell Biol 11 (5) (1999) 549–553. [PubMed: 10508654]

[39]. Boettner B, Van Aelst L, The Rap GTPase activator Drosophila PDZ-GEF regulates cell shape in epithelial migration and morphogenesis, Mol. Cell. Biol 27 (22) (2007) 7966–7980. [PubMed: 17846121]

[40]. Huelsmann S, et al., The PDZ-GEF dizzy regulates cell shape of migrating macro-phages via Rap1 and integrins in the Drosophila embryo, Development 133 (15) (2006) 2915–2924. [PubMed: 16818452]

[41]. Wairkar YP, et al., Unc-51 controls active zone density and protein composition by downregulating ERK signaling, J. Neurosci 29 (2) (2009) 517–528. [PubMed: 19144852]

[42]. Da-som Yang SR, The axon guidance function of Rap1 small GTPase is independent of PlexA RasGAP activity in Drosophila, Dev. Biol 418 (2) (2016) 258–267. [PubMed: 27565025]

[43]. Beck ES, et al., Regulation of fasciclin II and synaptic terminal development by the splicing factor beag, J. Neurosci 32 (20) (2012) 7058–7073. [PubMed: 22593074]

[44]. James Ashley MP, Fasciclin II signals new synapse formation through amyloid precursor protein and the scaffolding protein dX11/mint, J. Neurosci 25 (25) (2005) 5943–5955. [PubMed: 15976083]

[45]. Thelen K, et al., The neural cell adhesion molecule L1 potentiates integrin-dependent cell migration to extracellular matrix proteins, J. Neurosci 22 (12) (2002) 4918–4931. [PubMed: 12077189]

[46]. Hisata S, et al., Rap1-PDZ-GEF1 interacts with a neurotrophin receptor at late endosomes, leading to sustained activation of Rap1 and ERK and neurite outgrowth, J. Cell Biol 178 (5) (2007) 843–860. [PubMed: 17724123]

[47]. Martin KC, et al., MAP kinase translocates into the nucleus of the presynaptic cell and is required for long-term facilitation in Aplysia, Neuron 18 (6) (1997) 899–912. [PubMed: 9208858]

[48]. Ball RW, et al., Retrograde BMP signaling controls synaptic growth at the NMJ by regulating trio expression in motor neurons, Neuron 66 (4) (2010) 536–549. [PubMed: 20510858]

[49]. Xu B, et al., Strong association of de novo copy number mutations with sporadic schizophrenia, Nat. Genet 40 (7) (2008) 880–885. [PubMed: 18511947]

[50]. Xu B, et al., Elucidating the genetic architecture of familial schizophrenia using rare copy number variant and linkage scans, Proc. Natl. Acad. Sci. USA 106 (39) (2009) 16746–16751. [PubMed: 19805367]

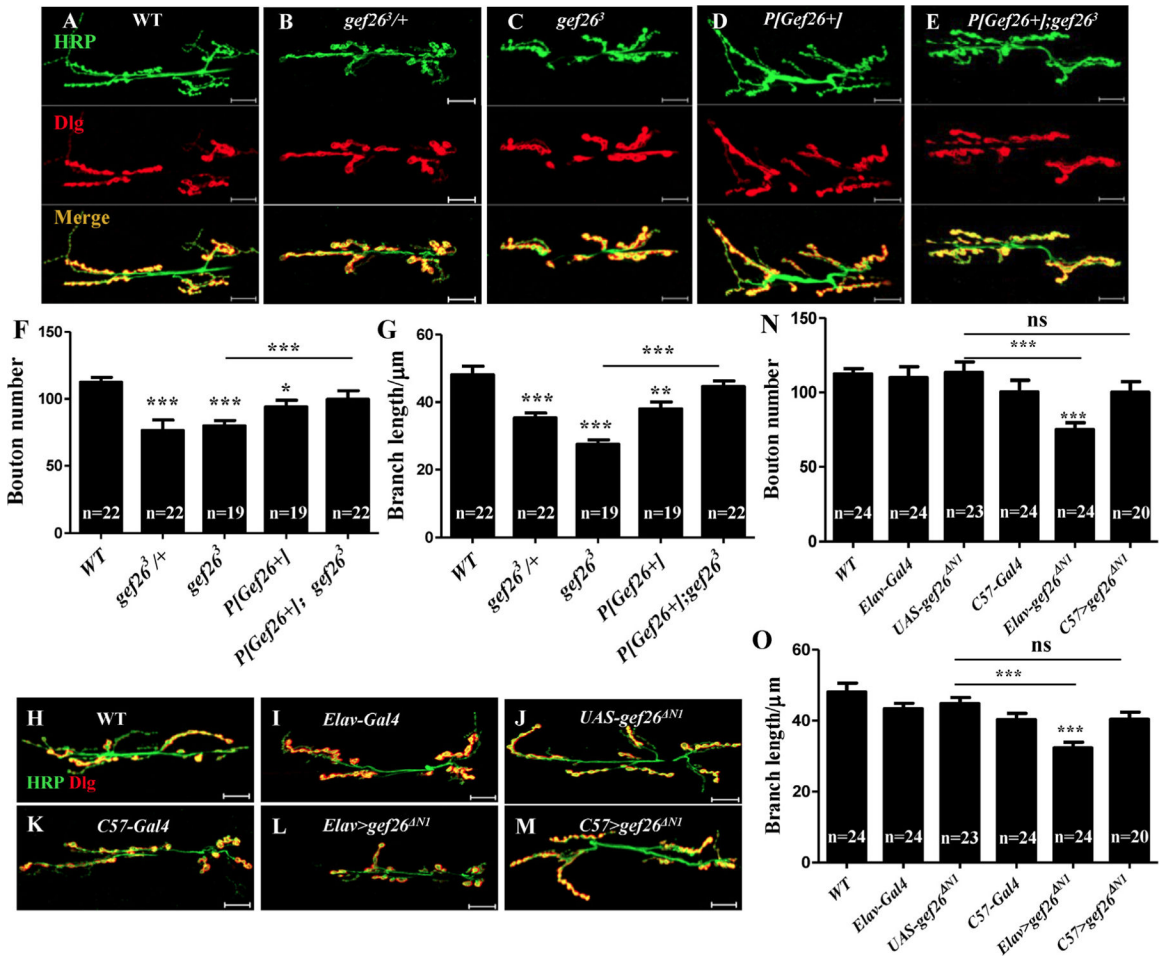

Fig. 1. Loss of Gef26 impairs NMJ morphology.

(A-E) Representative morphology of NMJ 6/7 of third-instar larvae labeled with anti-HRP and anti-Dlg antibodies in wild-type (WT), heterozygous mutant *gef26*^{3}*/+*, homozygous mutants *gef26*^{3} and *P[Gef26+]*, and the *P[Gef26+]* rescue line. *Scale bars= 20 μm.* (F-G) Quantification of bouton number and branch length of NMJ6/7 in the genotypes indicated in A-E. **p < 0.05*, ***p < 0.01*, ****p < 0.001.* (H-M) Representative morphology of NMJ 6/7 of third-instar larvae in *gef26*$^{\Delta N1}$ driven by pan–neuron-specific *Elav-Gal4* and muscle-specific *C57-Gal4*, as well as the *UAS* line and *Gal4* lines. (N-O) Quantification of bouton number and branch length of NMJ6/7 in the genotypes indicated in H-M. ****p < 0.001*; *ns*, *not significant.*

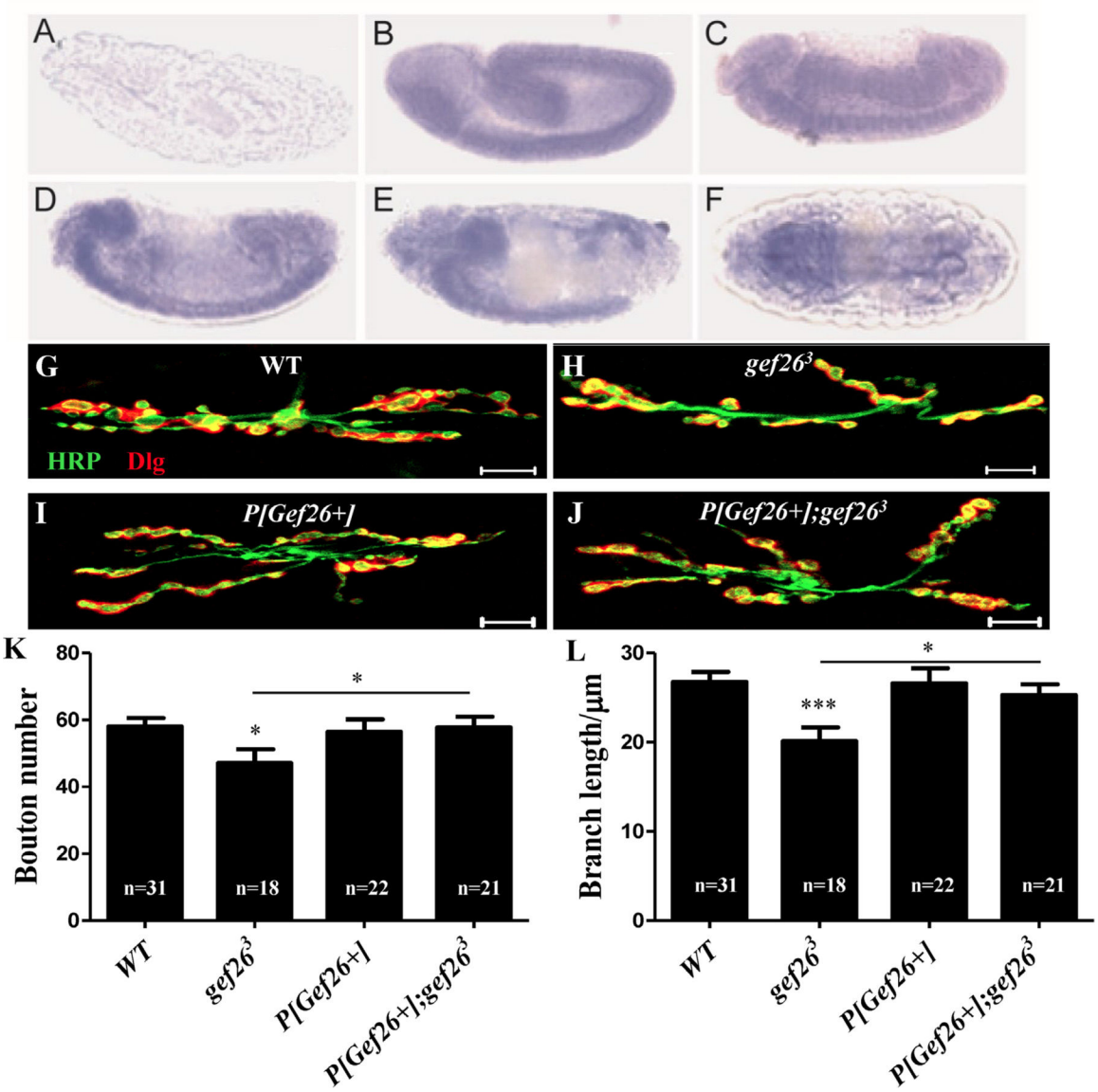

Fig. 2. Gef26 plays a role in NMJ development.

(A-F) RNA in situ hybridization showed spatial distribution of *Gef26* transcript in embryos. Embryos were oriented with anterior to the left. Lateral view of negative control showed no staining detected with sense probe (A). Lateral view of stage 13 (B), 14 (C), 15 (D), and 16 (E) embryos showed staining in the developing brain and ventral nerve cord (VNC). (F) Dorsal view of a stage 16 embryo showed expression of *Gef26* on ventral nerve cord. (G-J) Representative morphology of NMJ 6/7 of second-instar larvae in WT, *gef26*^{3}, *P[Gef26+]*, and the rescue line. *Scale bars = 10 μm.* (K-L) Quantification of bouton number and branch length of NMJ6/7 in the indicated lines in G-J. **p < 0.05, ***p < 0.001.*

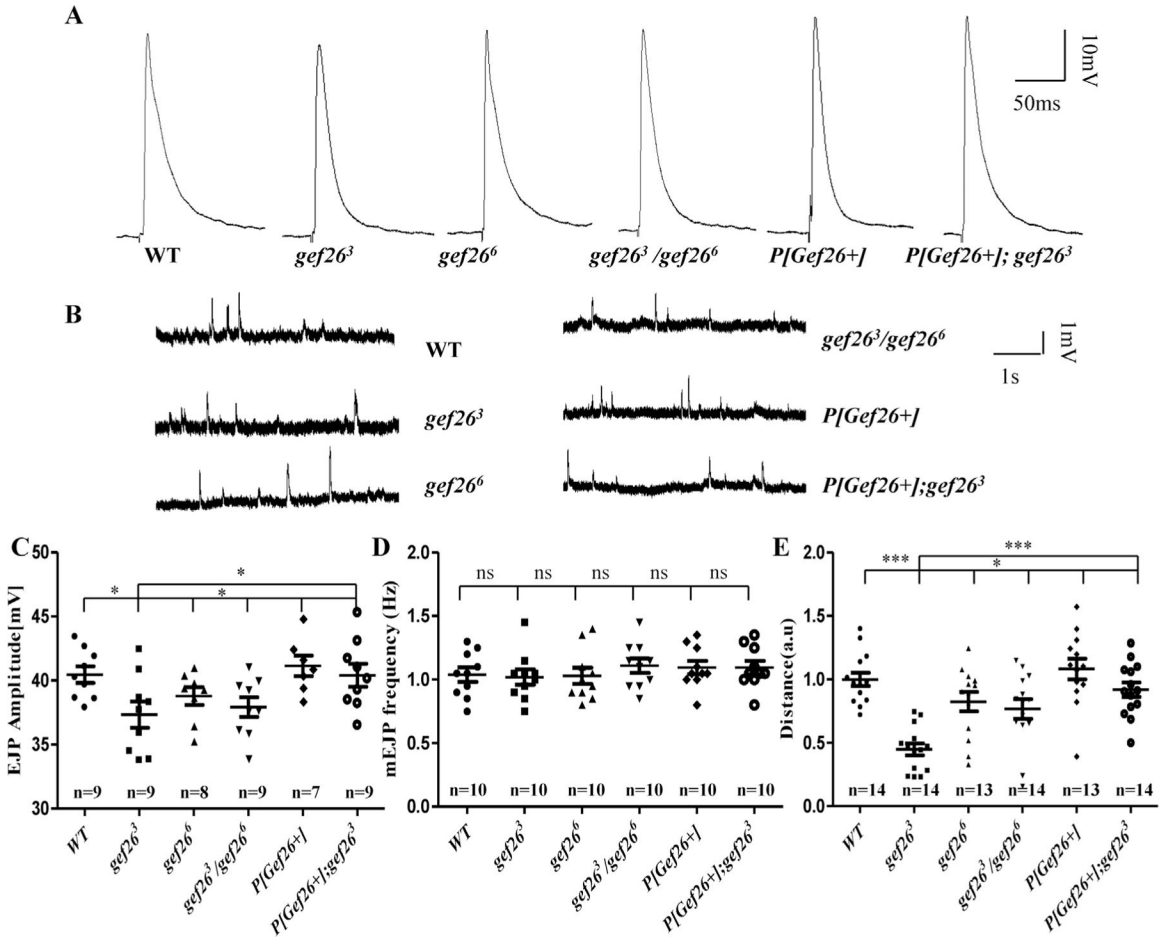

Fig. 3. Functional defects in Gef26 mutants.

(A) Representative traces of excitatory junction potentials (EJPs) at muscle 6 of the third-instar larvae in WT, homozygous mutants *gef26*^{3} and *gef26*^{6} as well as their allelic combination *gef26*^{3}/*gef26*^{6}, *P[Gef26+]*, and the *P[Gef26+]* rescue line. (B) representative traces of mEJPs at muscle 6 of the third-instar larvae in WT, homozygous mutants *gef26*^{3} and *gef26*^{6} as well as their allelic combination *gef26*^{3}/*gef26*^{6}, *P[Gef26+],* and the *P[Gef26+]* rescue line. (C-D) Quantification of EJP amplitude and miniature EJP (mEJP) frequency in the genotypes indicated in A and B. **p < 0.05; ns, not significant.* (E) Quantification of a 30-s crawling distance of the third-instar larvae in WT; homozygous mutants, *gef26*^{3} and *gef26*^{6}, as well as their allelic combination *gef26*^{3}/*gef26*^{6}, *P[Gef26+]*, and the *P[Gef26+]* rescue line (*a.u.*, arbitrary unit). **p < 0.05; ***p < 0.001.*

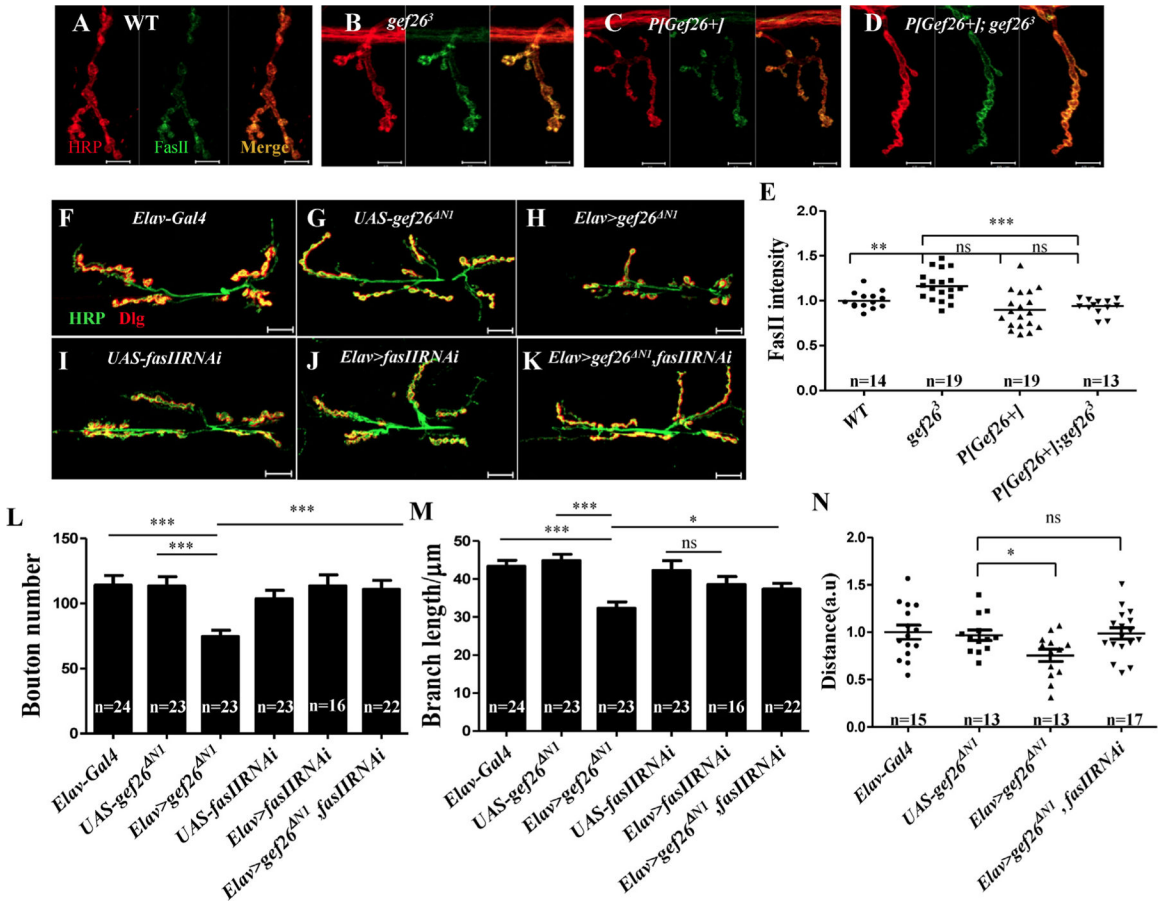

Fig. 4. Increased FasII is responsible for Gef26-associated NMJ morphogenesis.

(A-D) Representative images of NMJ4 of third-instar larvae labeled with anti-HRP and anti-FasII antibodies in WT, *gef26*^{3}, *P[Gef26+]*, and the rescue line. *Scale bars= 10 μm*. (E) Quantification of FasII intensity at NMJ4 in the genotypes indicated in A-D. ***p < 0.01*; ****p < 0.001*; *ns*, *not significant*. (F-K) Representative morphology of NMJ 6/7 of the third-instar larvae labeled with anti-HRP and anti-Dlg antibodies in *Elav-Gal4*, *fasIIRNAi* driven by *Elav-Gal4*, and *gef26*$^{\Delta N1}$ driven by *Elav-Gal4* as well as their *UAS* lines, and *Elav-Gal4*–driven *fasIIRNAi* and *gef26*$^{\Delta N1}$ simultaneously. *Scale bars= 20 μm*. (L-M) Quantification of bouton number and branch length of NMJ6/7 in the genotypes indicated in F-K. **p < 0.05*; ****p < 0.001*; *ns*, *not significant*. (N) Quantification of a 3-min crawling distance of the third-instar larvae in *Elav-Gal4*, *UAS-gef26*$^{\Delta N1}$, *Elav-Gal4*–driven *gef26*$^{\Delta N1}$ and *Elav-Gal4*–driven *fasIIRNAi* and *gef26*$^{\Delta N1}$ simultaneously. **p < 0.05; ns, not significant.*

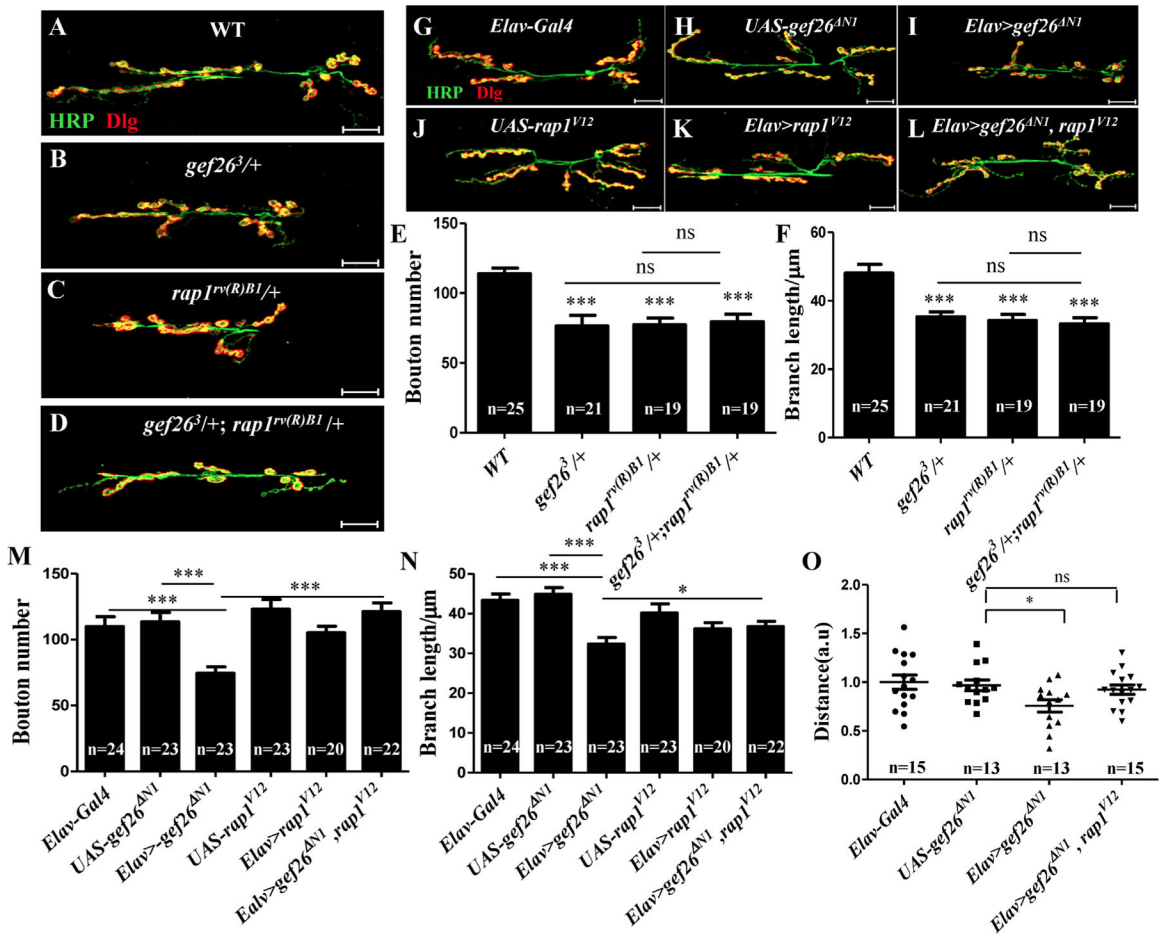

Fig. 5. Gef26 targets Rap1 in NMJ morphology.

(A-D) Representative morphology of NMJ 6/7 of the third-instar larvae labeled with anti-HRP and anti-Dlg antibodies in WT, heterozygotes of *gef26*^{3} and *rap1*$^{rv(R)B1}$, and *gef26*^{3}*/+ ;rap1*$^{rv(R)B1}$ */+* combining these two heterozygous mutants. *Scale bars= 20 μm*. (E-F) Quantification of bouton number and branch length of NMJ6/7 in the genotypes indicated in A-D. ** **p < 0.001*; *ns*, *not significant*. (G-L) Representative morphology of NMJ 6/7 of the third-instar larvae labeled with anti-HRP and anti-Dlg antibodies in *Elav-Gal4*, the sustained active form of Rap1; *rap1*^{V12} driven by *Elav-Gal4;* and *gef26*$^{\Delta N1}$ driven by *Elav-Gal4*; their *UAS* lines; and *rap1*^{V12} together with *gef26*$^{\Delta N1}$ driven by *Elav-Gal4* simultaneously. *Scale bars= 20 μm*. (M-N) Quantification of bouton number and branch length of NMJ6/7 in the genotypes indicated in G-L. **p < 0.05, ***p < 0.001*. (O) Quantification of a 3-min crawling distance of the third-instar larvae in *Elav-Gal4*, *UAS-gef26*$^{\Delta N1}$, *Elav-Gal4*–driven *gef26*$^{\Delta N1}$ and *Elav-Gal4*–driven *rap1*^{V12} and *gef26*$^{\Delta N1}$ simultaneously. **p < 0.05; ns, not significant.*

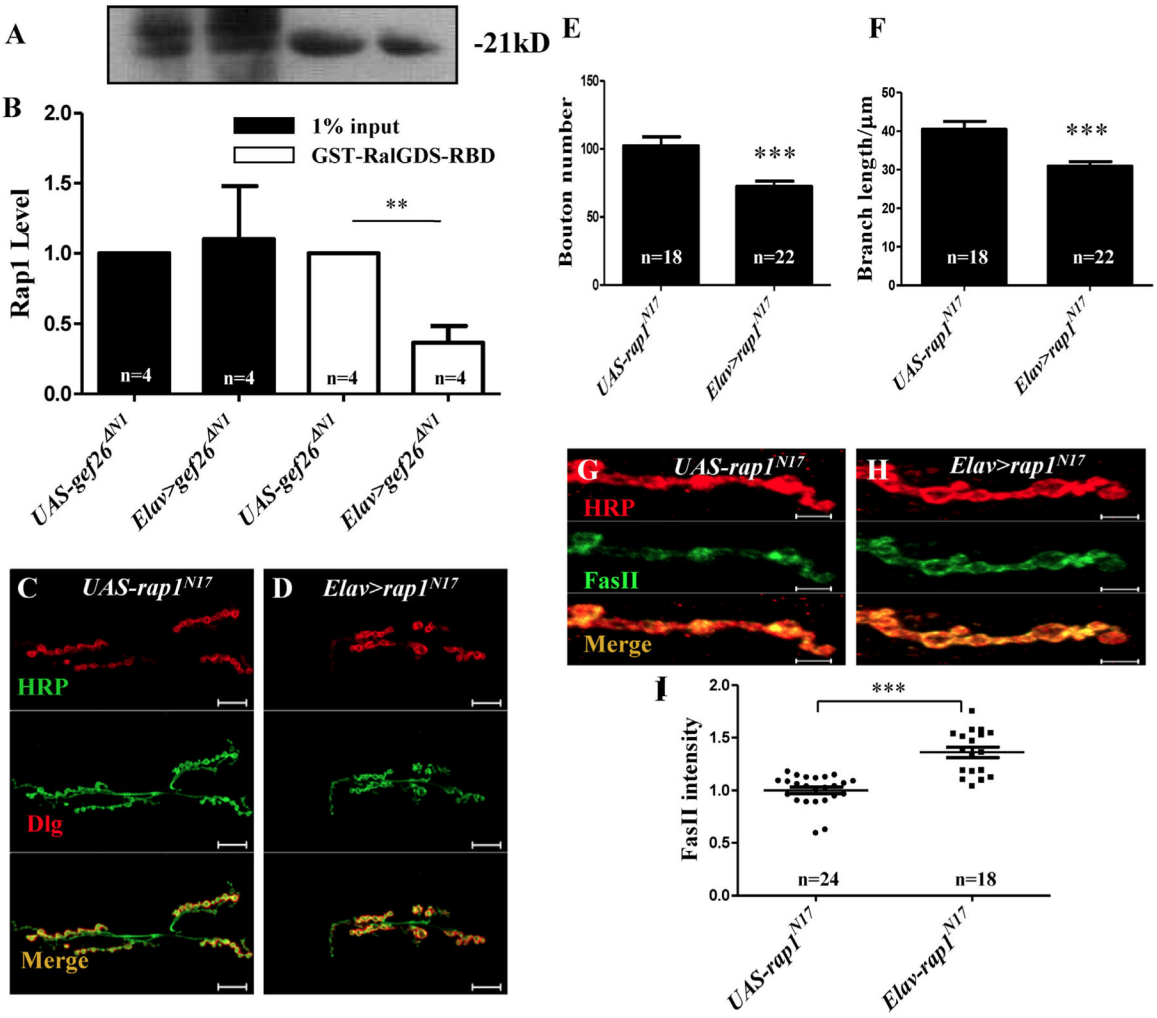

Fig. 6. Gef26 regulates Rap1 activity in nerves.

(A-B) GST pull-down of activated small GTPase. A GST-fusion protein of the Rap1-binding domain (RBD) from human RalGDS together with glutathione agarose resin was applied to specifically pull down activated Rap1. Input corresponds to 1% of total lysate prior to GST pull-down. The predicted size of Rap1 in *Drosophila* is about 21 kD. (A) Western blot analyses of active Rap1 obtained by GST pull-down of Rap1-GTP in adult head of *UAS-gef26*$^{\Delta N1}$ and *Elav-Gal4–driven gef26*$^{\Delta N1}$. (B) Quantification of amount of active Rap1 obtained by GST pull-down of Rap1-GTP in the genotypes indicated in A. Black bar indicates 1% input of total lysates and white bar indicates disposed with GST-RalGDS-RBD. *$^{**}p < 0.01$*. (C-D) Representative morphology of NMJ 6/7 of the third-instar larvae labeled with anti-HRP and anti-Dlg antibodies in dominant-negative form of Rap1, *Elav-Gal4–driven rap1*^{N17}, and the *UAS* line. *Scale bars= 20 μm*. (E-F) Quantification of bouton number and branch length of NMJ6/7 in the genotypes indicated in C-D. *$^{***}p < 0.001$*. (G-H) Representative images of NMJ 4 of third-instar larvae labeled with anti-HRP and anti-FasII antibodies in *Elav-Gal4–driven rap1*^{N17} and the *UAS* line. *Scale bars= 5 μm*. (I) Quantification of FasII intensity at NMJ4 in the genotypes indicated in G-H. *$^{***}p < 0.001$.*

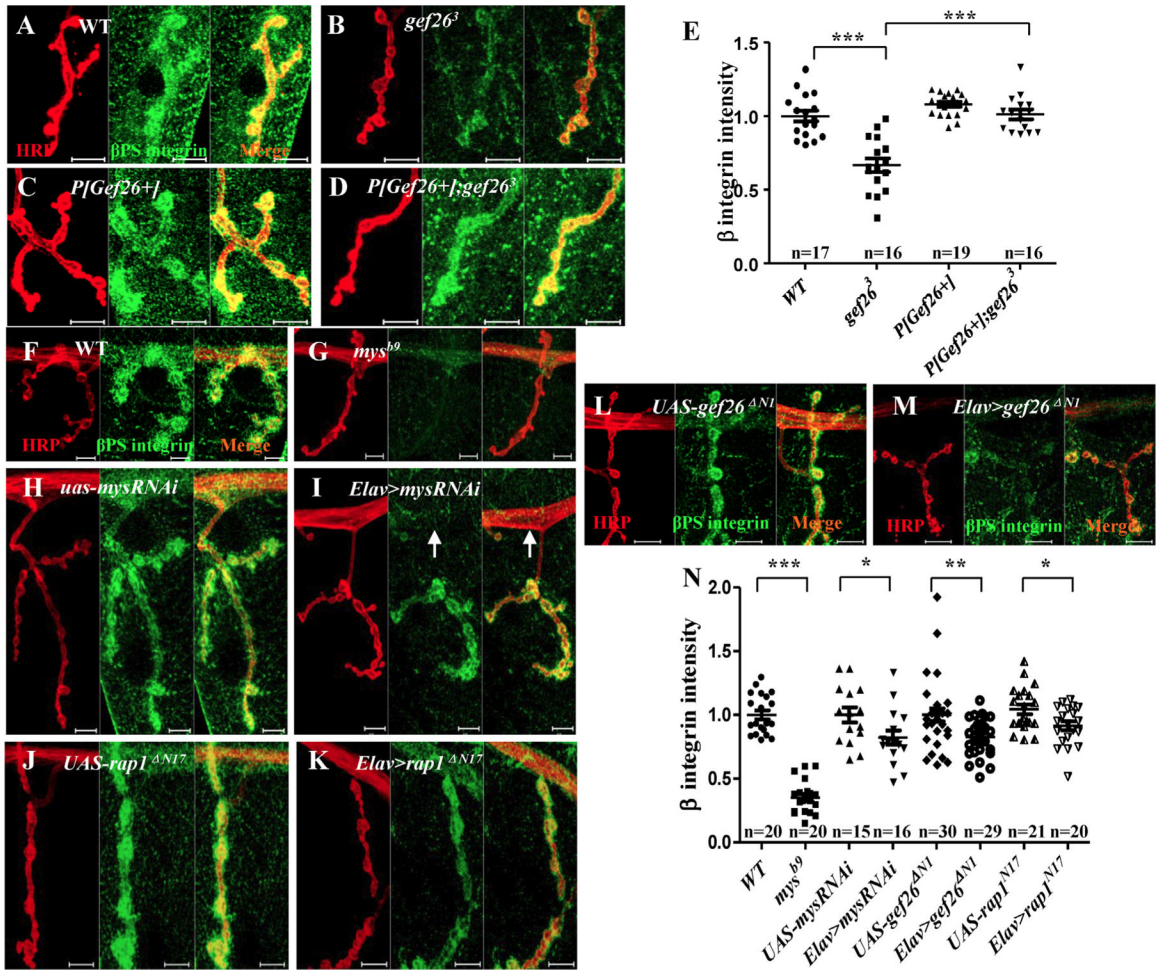

Fig. 7. Gef26 regulates synaptic FasII level through reducing integrin.

(A-D) Representative images of NMJ4 of third-instar larvae labeled with anti-HRP and anti-βPS antibodies in WT, *gef26*^{3}, *P[Gef26 +]*, and the rescue line. *Scale bars= 10 μm.* (E) Quantification of βPS intensity at NMJ4 in the genotypes indicated in A-D. ** **p < 0.001.* (F-M) Representative images of NMJ4 of third-instar larvae labeled with anti-HRP and anti-βPS antibodies in WT, *Mys* mutant *mys*^{b9}, *UAS-mysRNAi*, *Elav-Gal4–driven mysRNAi*, *UAS-gef26*$^{\Delta N1}$, *Elav-Gal4–driven gef26*$^{\Delta N1}$, *UAS-rap1*^{N17}, and *Elav-Gal4–driven rap1*^{N17}. *Scale bars= 10 μm.* Arrow indicates the clearly decreased βPS integrin level in the axon. (N) Quantification of βPS fluorescence intensity at NMJ4 in the genotypes indicated in F-M. **p < 0.05, **p < 0.01, ***p < 0.001.*